Supplementary Materials for the paper: CFD simulation of the BS 8414 test for Cladding Applications

Zhaozhi Wang, Fuchen Jia, Edwin R Galea*, John Ewer,
*Corresponding Author: e.r.galea@gre.ac.uk

Fire Safety Engineering Group, Centre for Safety, Resilience and Protective Security, University of Greenwich, Old Royal Naval College, 30 Park Row, Greenwich, LONDON SE10 9LS, UK

This document presents supplementary material for [S1] relating to, the HRR adopted for the wood crib fire in the analysis (see Section S1), HRR contribution from the burning of limited combustible materials (see Section S2), HRRs adopted for other cladding materials (see Section S3), details of the mesh independence study (see Section S4), detailed depiction of predicted and measured temperature profiles (see Section S5), description of cavity temperatures for the cavity size analysis (see Section S6), details of the window pod (see Section S7), and details of the material properties sensitivity analysis (see Section S8).

S1 HRR approach for wood crib fires

The fire source in BS 8414 test is a wood crib inside the fire chamber to represent a compartment fire breaking through a window to allow ejected flames to threaten the exterior cladding surface. British Standard BS 8414 [S2, S3] allows a large range of wood crib peak HRR, ranging from 2.5 MW to 3.5 MW. This wide range in HRR is not ideal for a fire test standard as the outcome of the test could be dependent on the fire size achieved in a particular test and hence the repeatability of the test is questionable. For modelling purposes, it is essential to have a reasonable HRR representing the wood crib combustion that can consistently be used in BS 8414 simulations, such as those presented in [S1].

A series outdoor fire tests according to the BS 8414 standard have been performed to determine fire performance of different cladding systems by Bjegović et al [S4]. In these tests, the mass of the fire source was measured during the test by applying load cells below each leg of the table onto which the wood crib was placed. The HRRs based on the mass loss rates are estimated and presented in Figure S1. It should be noted that these tests were performed outdoors with wind speed in the range of 2.2 m/s - 4.5 m/s. As a result, the peak HRRs are around 3.5-4.0 MW. An indoor free burning (without being confined in a BS 8414 chamber) of a BS 8414 wood crib [S5] also generates a high HRR. Without the impact of wind, the indoor BS 8414 wood crib fire produces a HRR of approximate 2.5 MW [S6].

In addition to the seven DCLG BS 8414 fire tests of various wall cladding systems [S7], DCLG BS 8414 test 8 has been conducted without a cladding system. Unfortunately, the HRR for this wood crib fire test is not reported. The wood crib HRR for the BS 8414 model used to simulate the DCLG BS 8414 fire tests [S2] is determined by satisfying the following conditions:

- The HRR is as close as possible to that produced by the BS 8414 test without cladding materials [S6].
- The simulated fire plume with the selected HRR should match that observed in the DCLG BS 8414 test 8, in which the fire load is the wood cribs only (without cladding system).
- For a scenario without cladding materials (i.e., the wood crib is the only fire source), the simulated level 2 external temperatures should be in reasonably good agreement

with the data in the DCLG tests at the peak crib fire, in which the heat contribution from the cladding system is still minor (i.e., test 6).

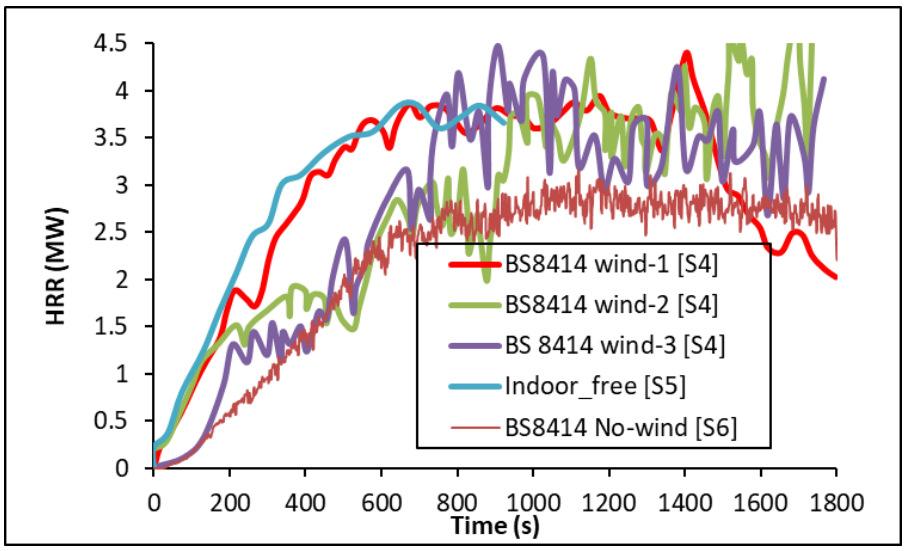

Fig. S1. HRRs from the combustion of BS 8414 cribs.

Three wood crib fire scenarios are considered here, 2.5 MW, 3.0 MW and 3.5 MW respectively. As seen in Fig. S2 and Fig. S3, the fire plume in the simulation of the 2.5 MW wood crib fire provides the best approximation to that observed in the DCLG BS 8414 test 8 among the three crib fire scenarios.

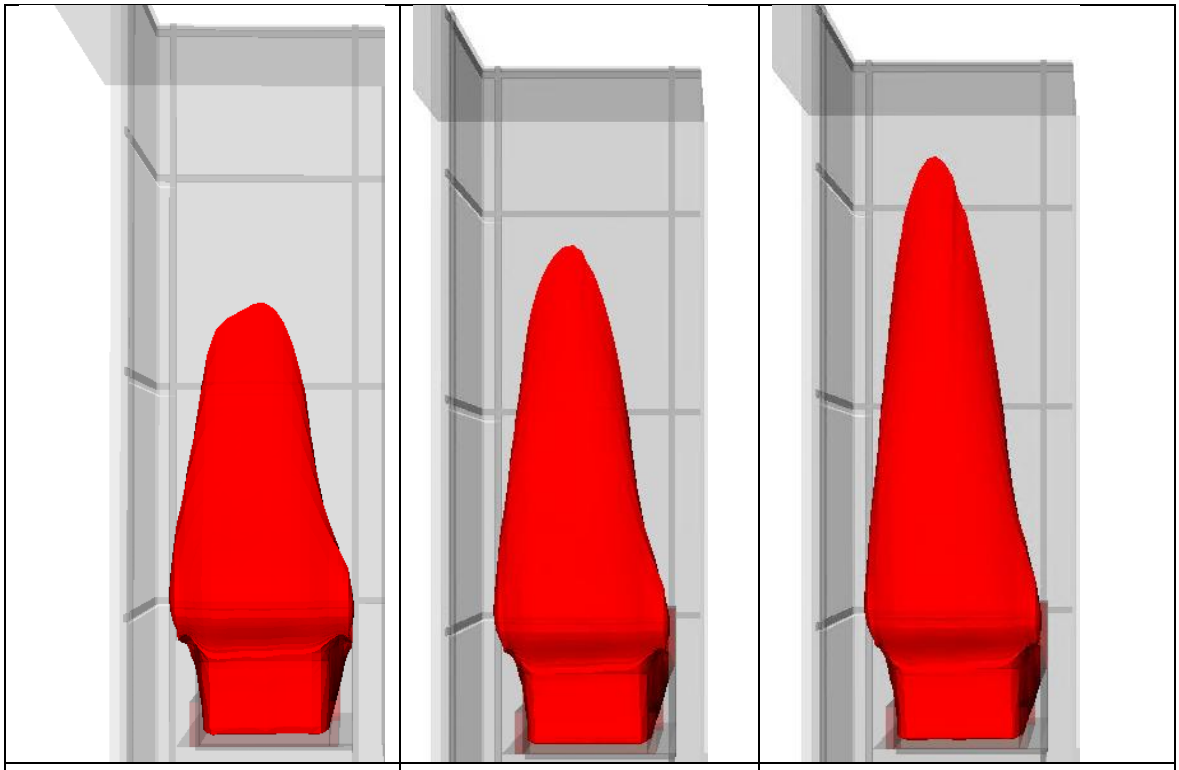

burning rate of 2.5 MW	burning rate of 3.0 MW	burning rate of 3.5 MW

Fig. S2. The simulated crib fire plumes at steady state (represented using the 525 ^{O}C temperature iso-surface) for various HRRs.

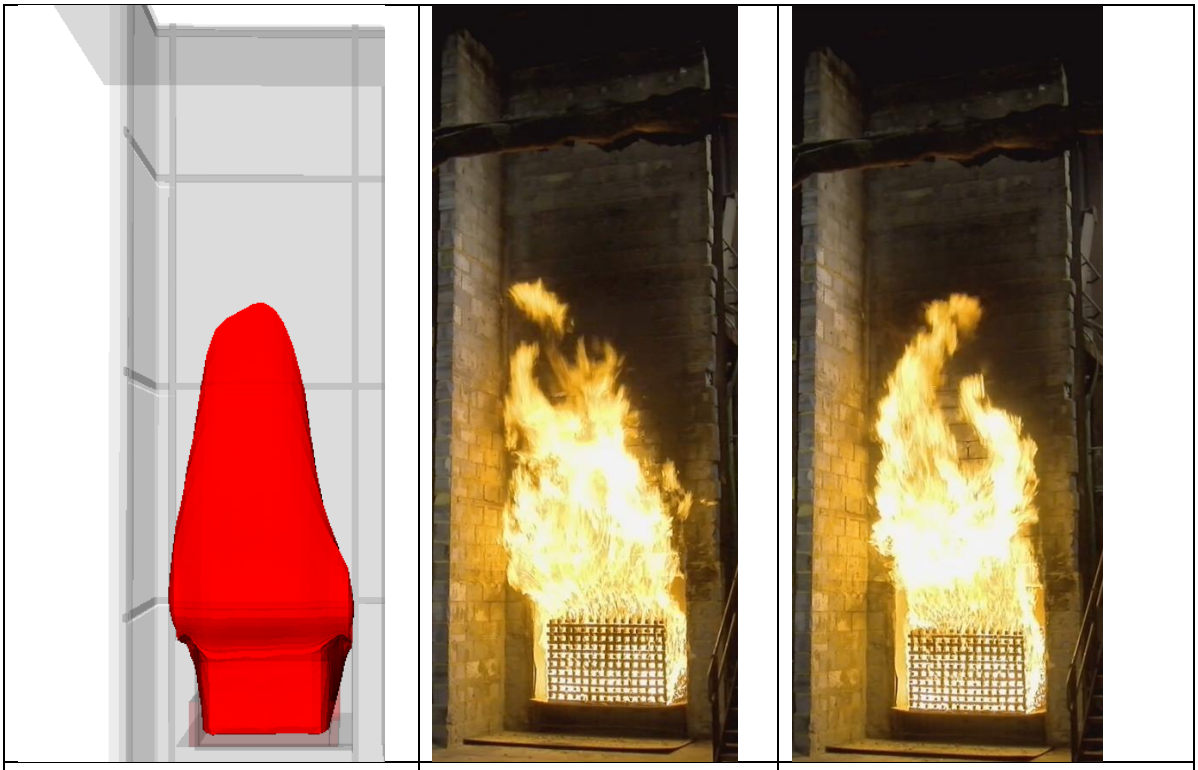

Fire flame (represented using the 525 ^{O}C temperature iso-surface) with burning rate of 2.5 MW	DCLG test 8 at 21 minutes 22 seconds	DCLG test 8 at 21minutes 24 seconds

Fig. S3. The simulated crib fire plume with a HRR of 2.5 MW and those from the DCLG BS 8414 test 8.

The simulated external horizontal temperature distributions at level 2 for the steady wood crib fire are compared in Fig. S4. The maximum temperatures are 350 ^{O}C, 443 ^{O}C and 513 ^{O}C for the 2.5 MW, 3.0 MW and 3.5 MW wood crib fire respectively. The simulated maximum temperature should be similar or less than the measured data in which the HRR from the burning of cladding materials is minor. DCLG BS 8414 test 6 consists of limited combustibility mineral as ACM core and stone wool as insulation. This test is simulated with a wood crib fire of 2.5 MW. The measured and simulated maximum external temperature at level 2 are presented in Fig. S5. In this case, sustained flaming due to the cladding fire is not seen until 9 minutes. The maximum measured level 2 temperature before 10 minutes is around 300 ^{O}C (Fig. S5) implies that the wood crib HRR does not exceeds 2.5 MW. Furthermore, the measured and simulated maximum external temperature at level 2 are in very good agreement during the entire half hour test (See Fig. S5) using the wood crib fire approach given in Fig. S6.

Therefore, the wood crib HRR presented in Fig. S6 is used in the BS 8414 model and the simulations of the seven DCLG cladding fires in this study [S1].

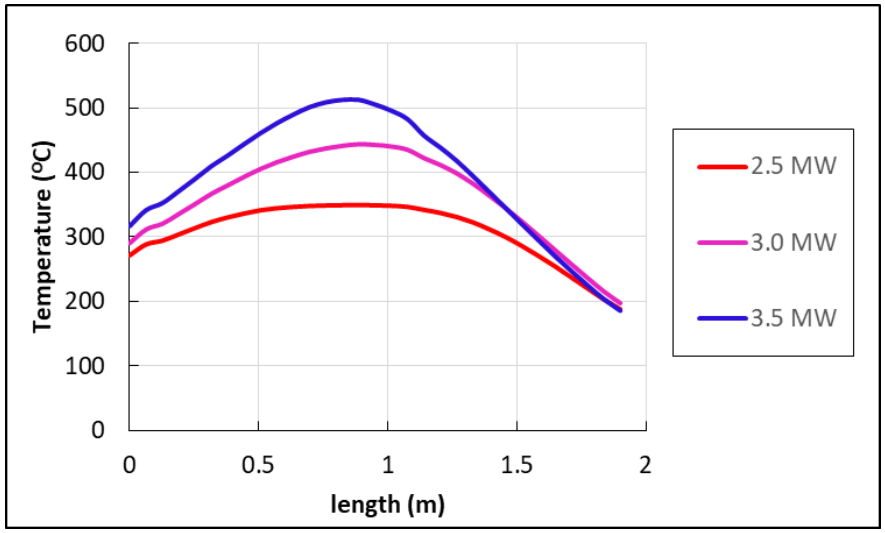

Fig. S4. Horizontal distributions of level 2 temperatures in the simulations with various wood crib fires.

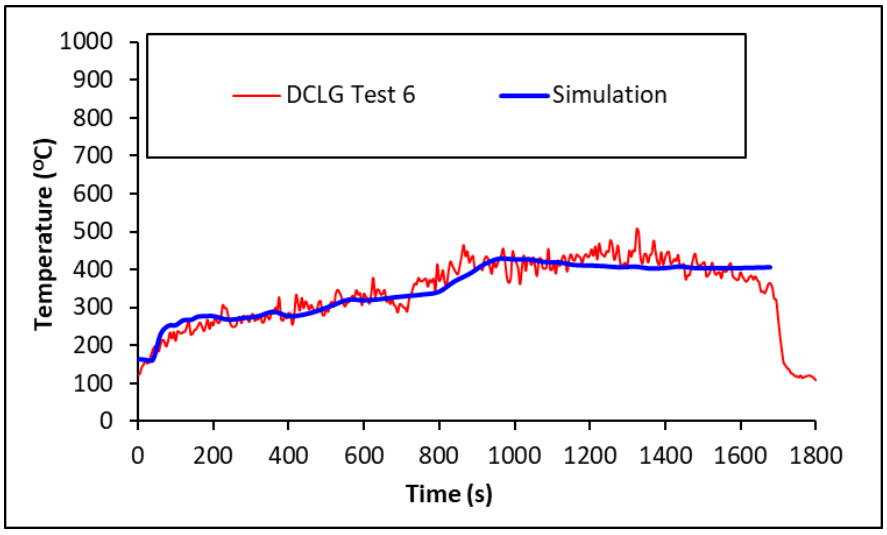

Fig. S5. Measured and simulated maximum external temperature at level 2 for DCLG test 6.

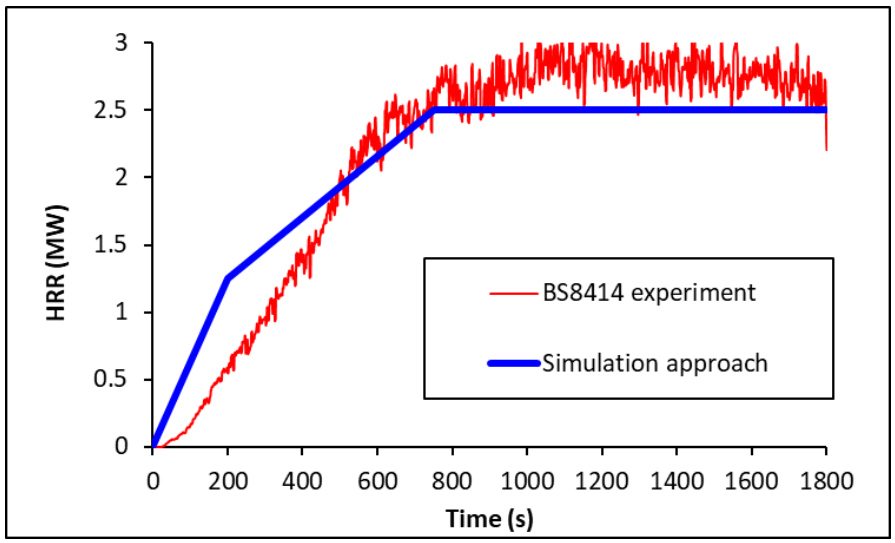

Fig. S6. Wood crib fire approach in the DCLG BS 8414 simulations (the experimental data is from [S6]).

S2 HRR from the limited combustibility material in BS 8414 DCLG test 5 fire simulation

DCLG test 5 and Test 6 include cladding systems incorporating ACM panels with limited combustibility core materials. Using the ignition temperature values of 550^{O}C and 480^{O}C for the surface and edge ignition criteria, the predicted HRR from the burning of limited combustibility material in the simulation of BS 8414 DCLG test 5 is depicted in Fig. S7. The HRR contribution from the burning of the limited combustibility material is no more than 0.023 MW throughout the simulation. This HRR contribution is less than 1% of the HRR of the wood crib fire source, which is much less than the accepted uncertainty for the wood crib HRR in the BS 8414 test protocol. Thus, the HRR contribution for the limited combustibility material, while using the 550^{O}C and 480^{O}C for the surface and edge ignition criteria, is so small, it is unlikely to significantly impact the results. Therefore, using the specified surface and edge ignition criteria is applicable for ACMs with a limited combustibility material core.

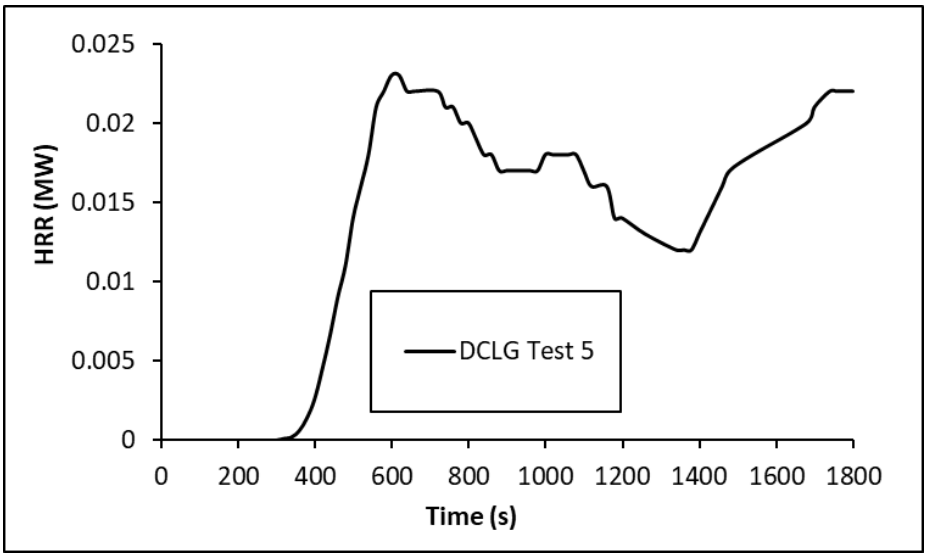

Fig. S7. Predicted HRR from the burning of the limited combustibility material in the simulation of BS 8414 DCLG test 5.

S3 HRRs for cladding materials

Presented in Figure S8 are the HRRs for each ACM core and insulation material used in this study [S1]. These data are the cone calorimeter data under an external heat flux of 50 kW/m^2 derived by McKenna et al. [S8].

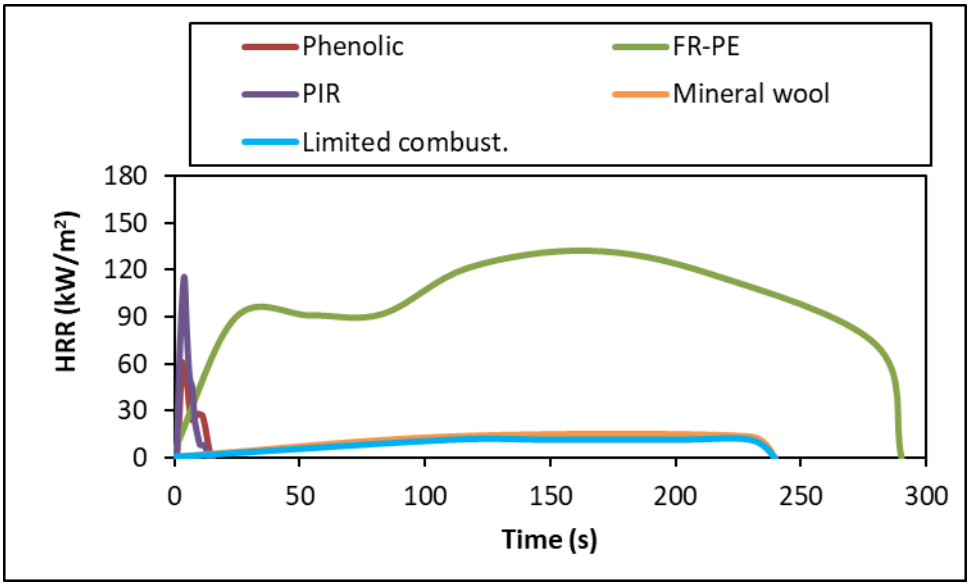

(a)

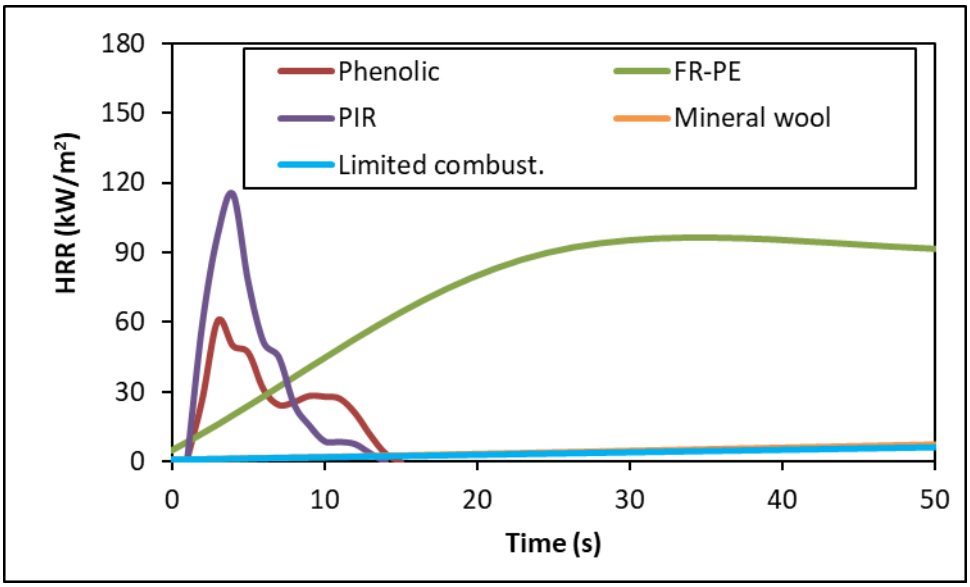

(b)

Fig. S8. HRRs of phenolic foam, FR PE, PIR, mineral wool and limited combustibility materials used in the DCLG BS 8414 simulations during (a) the whole burning process and (b) the first 50 seconds (to clearly show the curves for Phenolic and PIR) (derived from [S8]).

S4 Mesh sensitivity analysis

To assess the mesh sensitivity of the CFD simulations, two DCLG BS 8414 tests were simulated, test 1 with an early fail at 360 s and test 7 which just failed at 1525 s. Four mesh density cases were considered for DCLG BS 8414 test 1, with computational cells of 208539, 300348, 704850 and 1019424 respectively (See Table S1). While the average cell sizes are presented in Table S1, a non-uniform mesh is used, with a cell size of 0.0125 m inside the cavity (i.e., two cells each measuring 0.0125 m defining the horizontal cavity barrier (i.e., a total thickness of 0.025 m) and two cells each measuring 0.0125 m for the gap (which is 0.025

m wide) between the horizontal barrier and ACM back) is utilised for all the three mesh scenarios. As seen in Fig. S9(a), the simulated maximum external temperatures at Level 2 and in the cavity are almost identical in Mesh 1 and Mesh 2 with relatively coarse meshes. The simulated results in the two relatively fine mesh cases, Mesh 3 and Mesh 4 are almost identical too. As seen in Table S2, the predicted times for the rise of the external level 2 temperatures to exceed 600 ^{O}C are between 350 s and 380 s for the four mesh cases. Compared with the observed time of 360 s in the test, the prediction errors are within 5.6%. Similar mesh dependence predicted temperatures trends are also seen for the cavity temperature (Fig. S9(b)). The general agreement between the model predictions and experimental results are presented and discussed in the main paper, Section 3.4 [S1].

Table S1. Simulation cases for mesh sensitivity study.

Case	**Computational cells**	**Average cell size (m^3)**	**Simulated test**	**CPU time (h)**	
				840 s DCLG test 1 fire	**1800 s DCLG test 7 fire**
1	208,539 (51×87×47)	0.098×0.057×0.106	DCLG test 1	47	NA
2	300,348 (54×103×54)	0.093×0.049×0.093	DCLG tests 1, 7	71	117
3	704,850 (74×127×75)	0.068×0.039×0.067	DCLG tests 1, 7	192	214
4	1019424 (82×148×84)	0.061×0.034×0.060	DCLG test 1	276	NA

DCLG test 1 failed in the experiment due to the flame extending beyond the test facility at 360 s. In the simulations, the times for the flame to pass the top of the test facility are between 340 s and 360 s for the four mesh cases with relative errors from 0% to 5.6% respectively (Table S2). As seen in Fig. S10, the simulated fire plume when it passes the top of the test facility are quite similar for the four mesh cases. Almost identical burning locations at the derived termination times in the four mesh cases have also been obtained (Fig. S11).

Table S2. Observed and simulated key events from the coarse and fine mesh scenarios.

	Time for flame to extend beyond the test facility (s) (error %)		**Time for Level 2 temperature to exceed 600 ^{O}C (s) (error %)**	
	DCLG test 1	**DCLG test 7**	**DCLG test 1**	**DCLG test 7**
Experiment	360	1525	360	1490
Mesh 1	355 (1.4%)	NA	370 (2.8%)	NA
Mesh 2	360 (0%)	1360 (10.8%)	380 (5.6%)	1320 (11.4%)
Mesh 3	340 (5.6%)	1240 (18.7%)	355 (1.4%)	1160 (22.1%)
Mesh 4	340 (5.6%)	NA	350 (2.8%)	NA

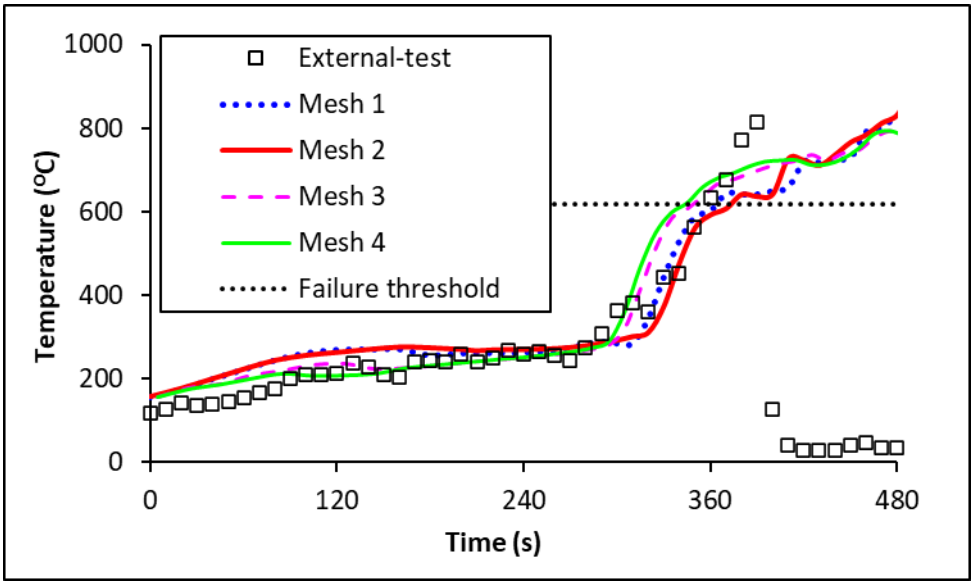

(a)

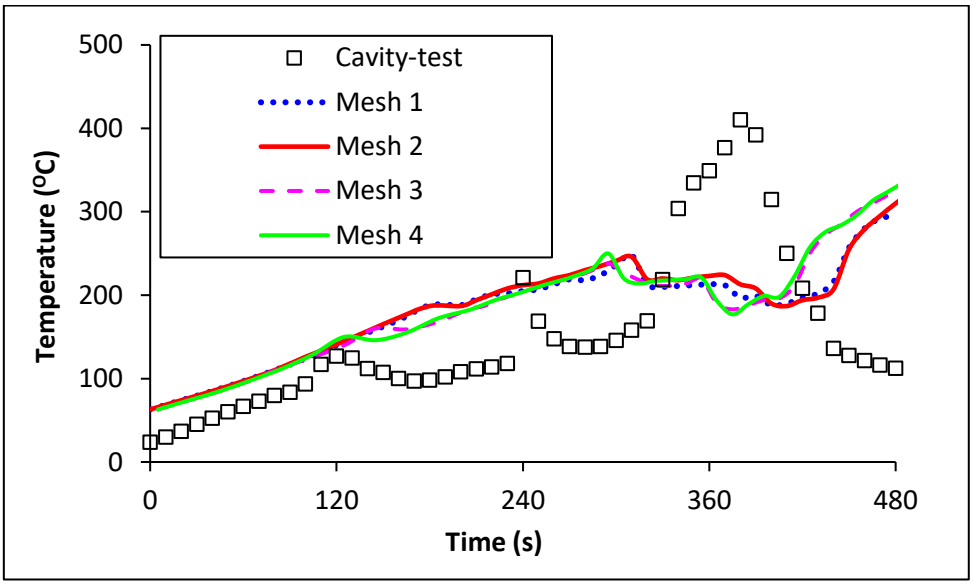

(b)

Fig. S9. Comparison of maximum external temperature at (a) external level 2 and (b) in Cavity between the measurement and simulations using four different mesh budgets for DCLG BS 8414 test 1.

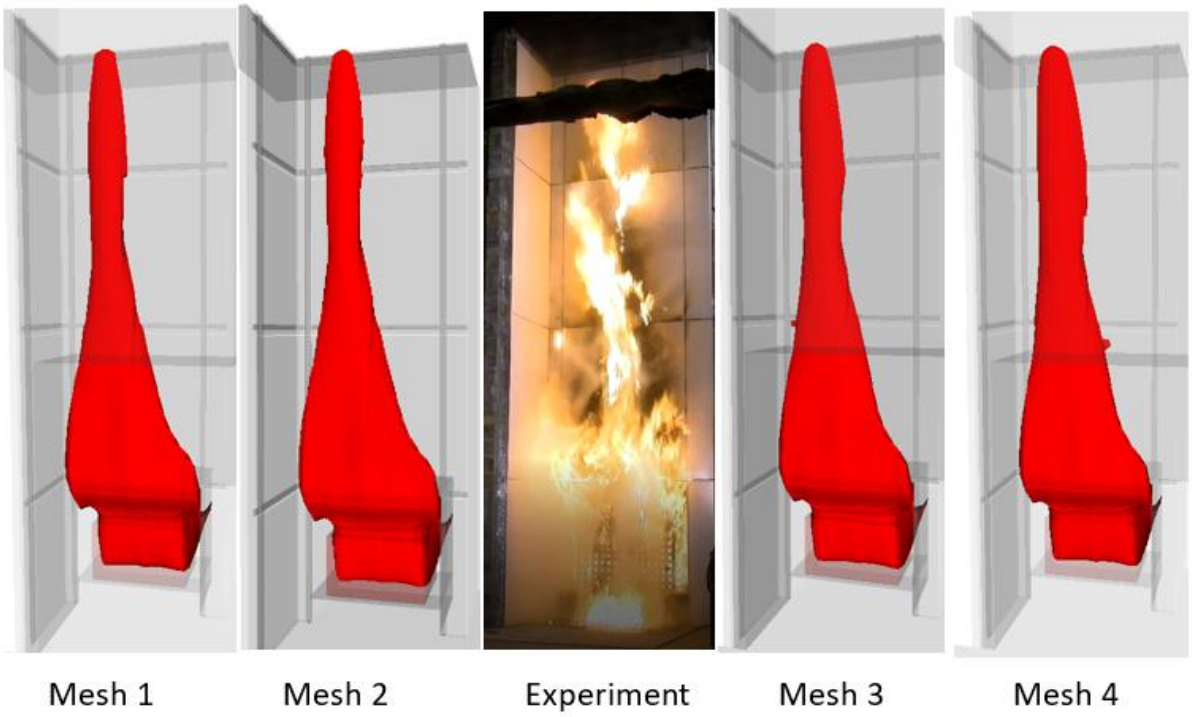

Fig. S10. Observed and predicted fire plumes at the time to fail in the simulations using four meshes respectively for DCLG test 1.

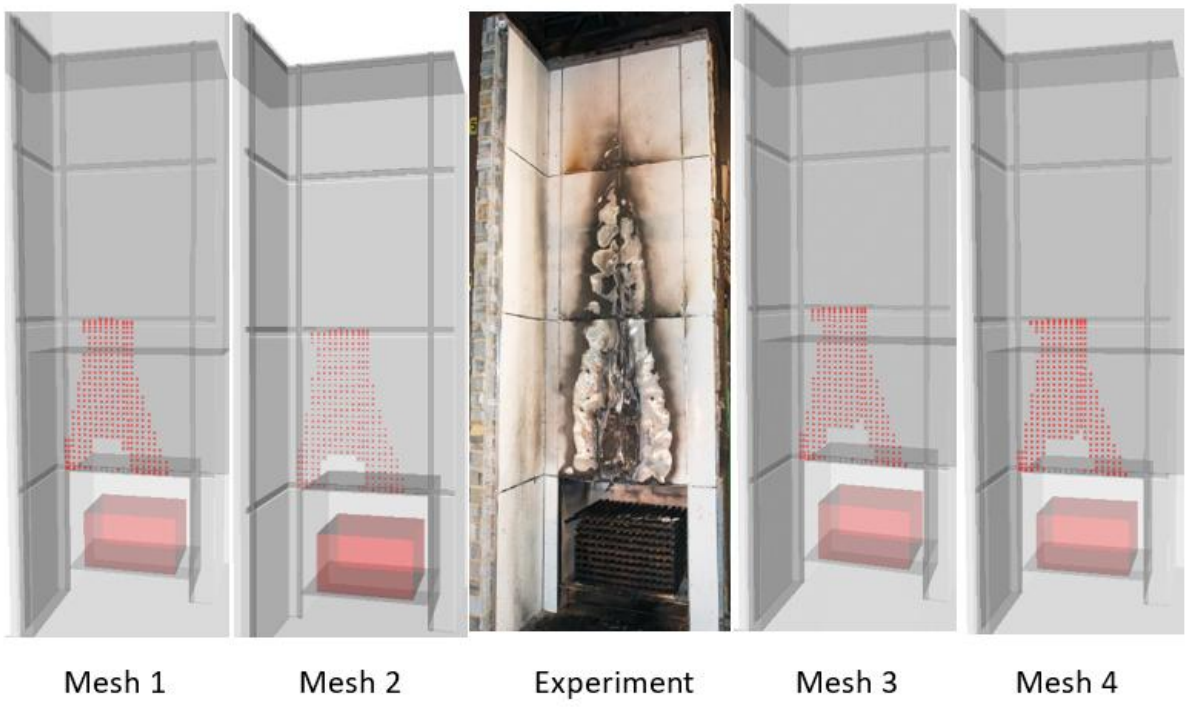

Fig. S11. Observed and predicted burning locations from the simulations using four meshes respectively for GCLG test 1.

DCLG test 7 has been simulated using Mesh 2 and Mesh 3. The time for the level 2 temperature to exceed the initial temperature by 600 ^{O}C is 1490 s in the test. The simulated times are 1320

s and 1160 s from the two mesh cases, with relative errors of 11.4% and 22.1% respectively (See Table S2 and Fig. S12). Almost identical temperature curves in the cavity have been produced by the two mesh cases. DCLG test 7 failed at 1525 s due to the flame extending beyond the test facility. In the simulations, the times for the flame to pass the top of the test facility are 1360 s and 1240 s, with relative errors 10.8% and 18.7% respectively (Table S2). The simulated fire plumes when it passes the top of the test facility are almost identical for the two mesh scenarios (Fig. S13). Although the cladding fire extends to similar locations at the derived termination times in the two mesh cases, a bigger burnt off ACM area in Mesh 2 than Mesh 3 is seen (Fig. S14).

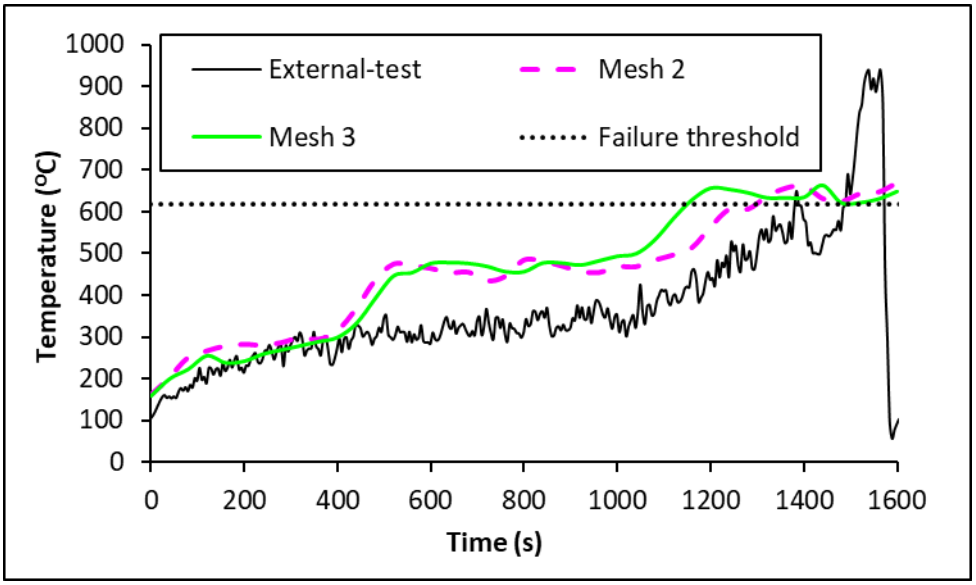

(a)

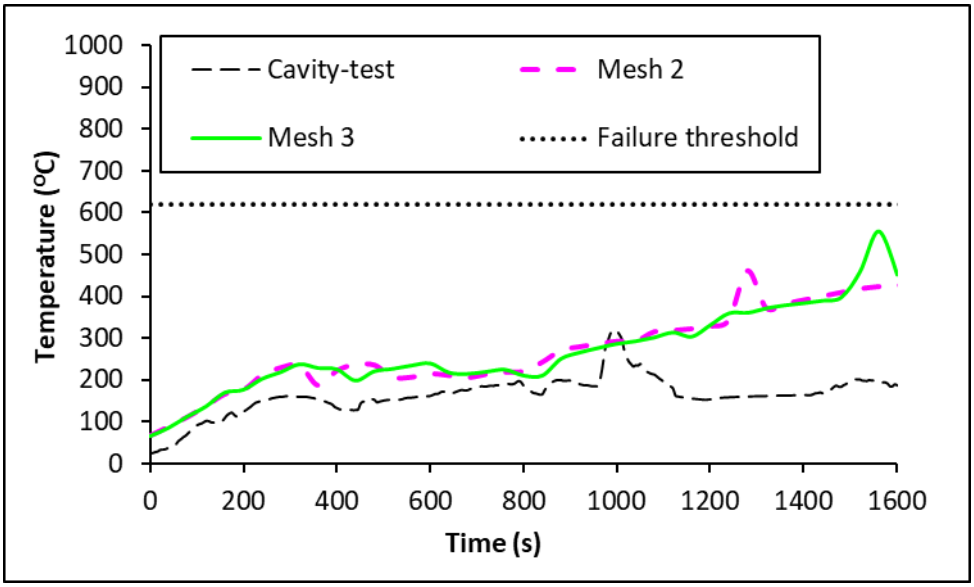

(b)

Fig. S12. Measured and simulated maximum temperature (a) external at level 2 and (b) in cavity as functions of time for DCLG BS 8414 test 7.

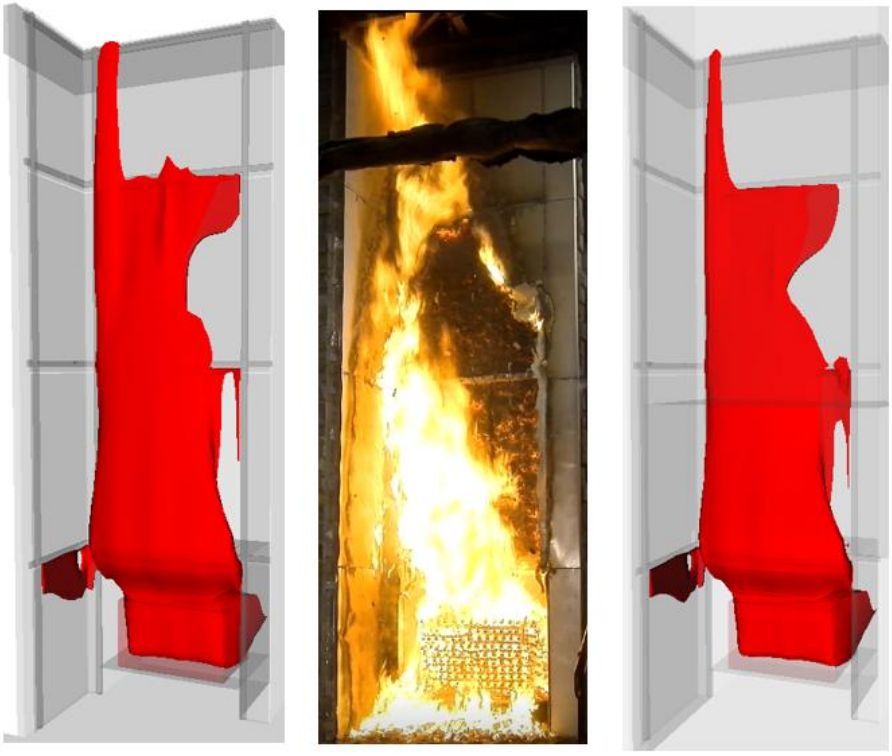

Fig. S13. Observed (middle) and predicted fire plumes at the time to fail in the simulations using the Mesh 3 (left) and Mesh 4 (right) meshes respectively for GCLG test 7.

Fig. S14. Observed (middle) and predicted burning locations from the simulations foe Mesh 3 (left) and Mesh 4 (right) respectively for DCLG test 7.

Overall, the simulations of DCLG test 1 using four meshes and the simulations of DCLG test 7 using two meshes, have successfully reproduced the same 'fail' test results and with the same causes as were observed in the tests. The prediction errors for the time to fail (due to the flame extending beyond the top of the test facility) are within 5.6% for test 1 and 18.7% for test 7. The prediction errors for the external level 2 temperature to exceed the initial temperature by 600 ^{O}C are within 5.6% for the four mesh cases for Test 1 and within 22.1% for mesh cases for Test 7. The simulations from the four mesh cases for the two tests have also produced similar temperature curves, flame shapes and burning locations, which all are comparable with the measured data or observation. Thus, while all the meshes would lead to the same conclusions, particularly in terms of pass/fail of the cladding system and the corresponding causes, considering the CPU time (Table S2), the relative coarse mesh, Mesh 2 (300,348 cells) was considered appropriate for the purposes of the study in the main paper [S1].

S5 Measured and predicted temperature profiles at Level 1 (external), Level 2 (external) and Level 2 (internal)

In the main paper [S1] the measured and predicted temperature profiles at each of the three thermocouples at each group location were presented on a single graph, resulting in three graphs each with six curves, see Fig. 5a for level 2 external, Fig. 5b for level 2 internal cavity and Fig. 5c for level 1 external. For improved clarity, presented in Fig. S15 to S17 are 9 graphs each with just two curves, the experimental and predicted temperature profile for a single thermocouple location.

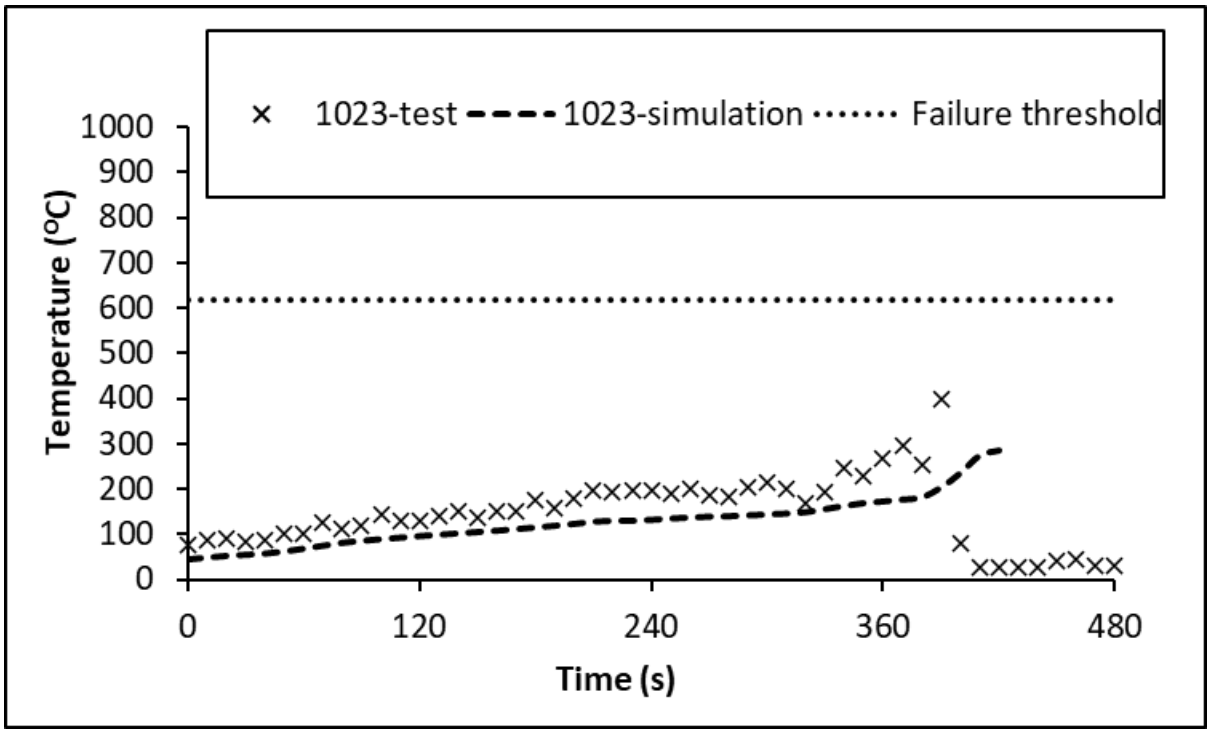

(a)

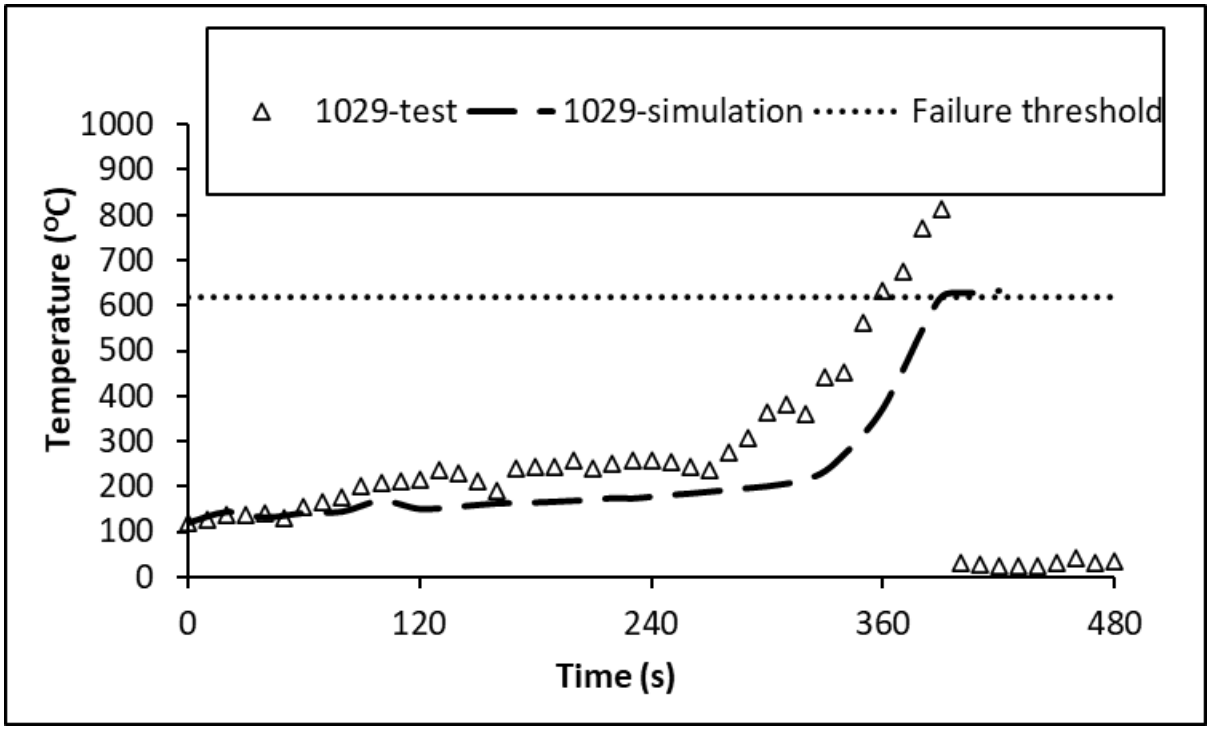

(b)

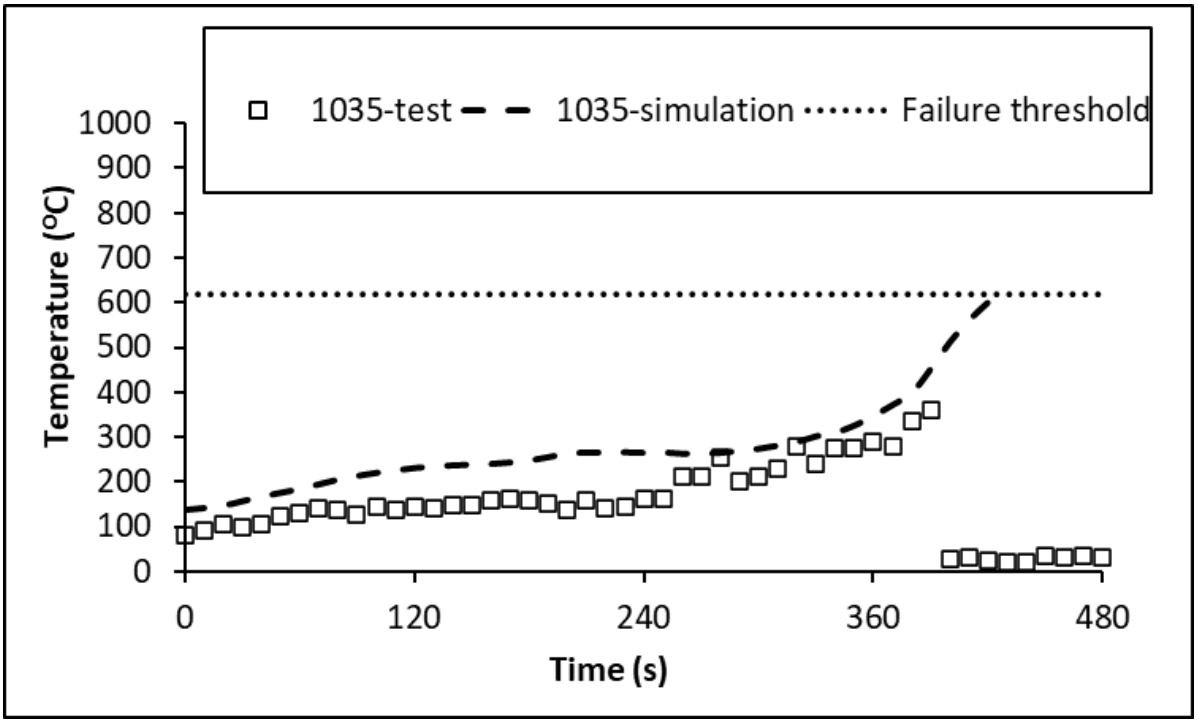

(c)

Fig. S15. Measured and predicted temperatures at external level 2 thermocouples (a) 1023; (b) 1029 and (c) 1035.

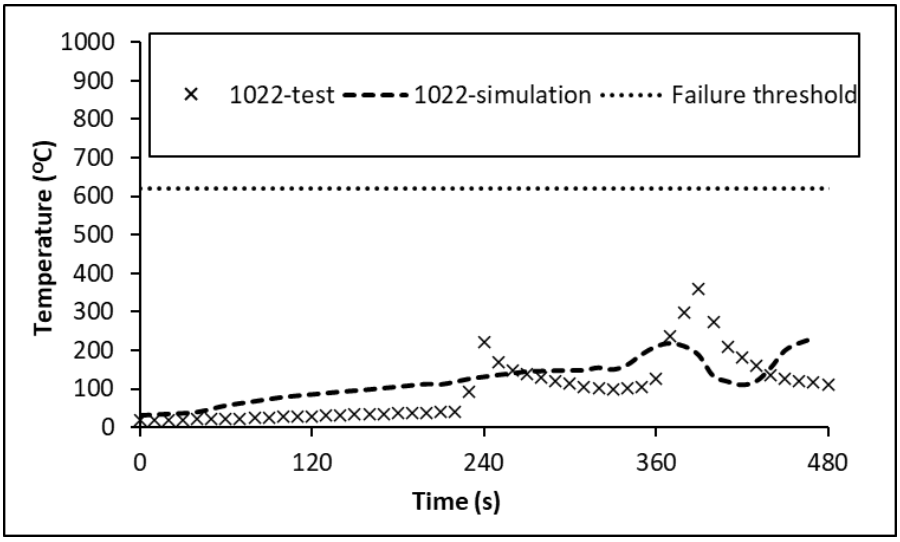

(a)

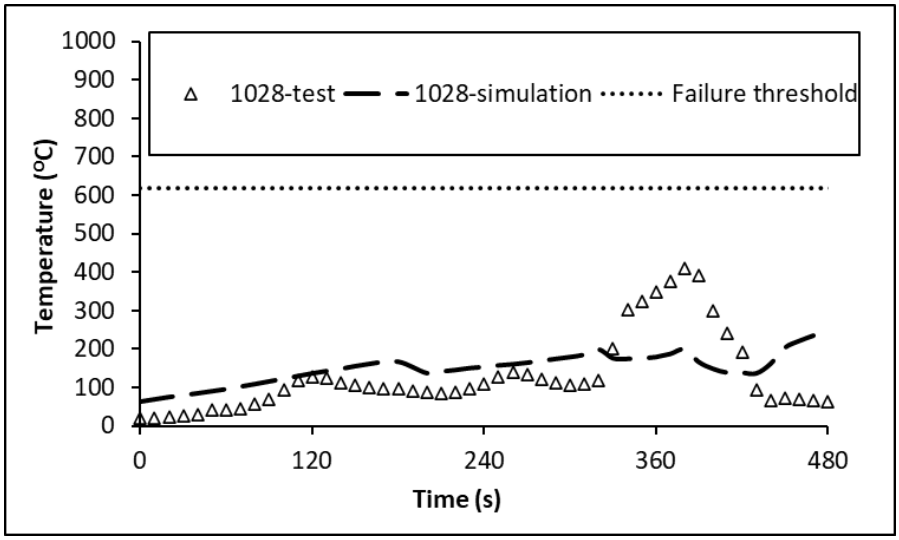

(b)

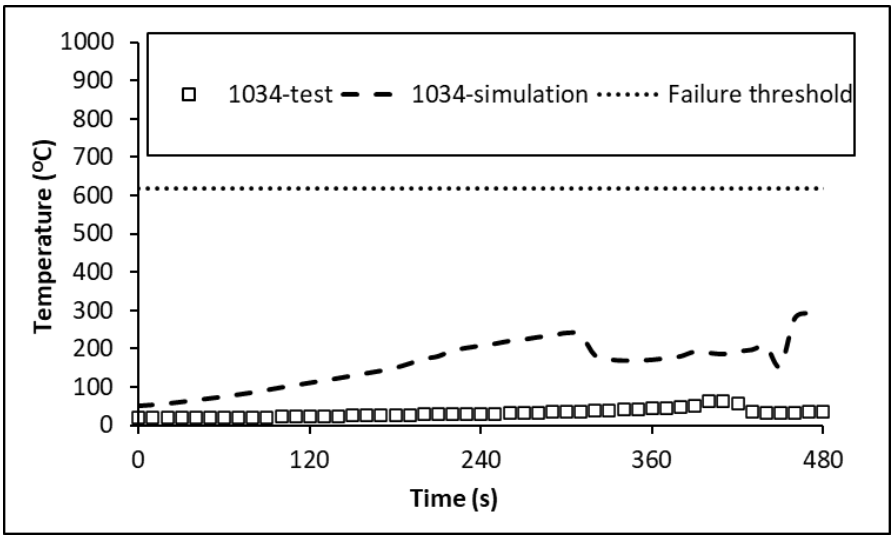

(c)

Fig. S16. Measured and predicted temperatures at cavity thermocouples (a) 1022; (b) 1028 and (c) 1034.

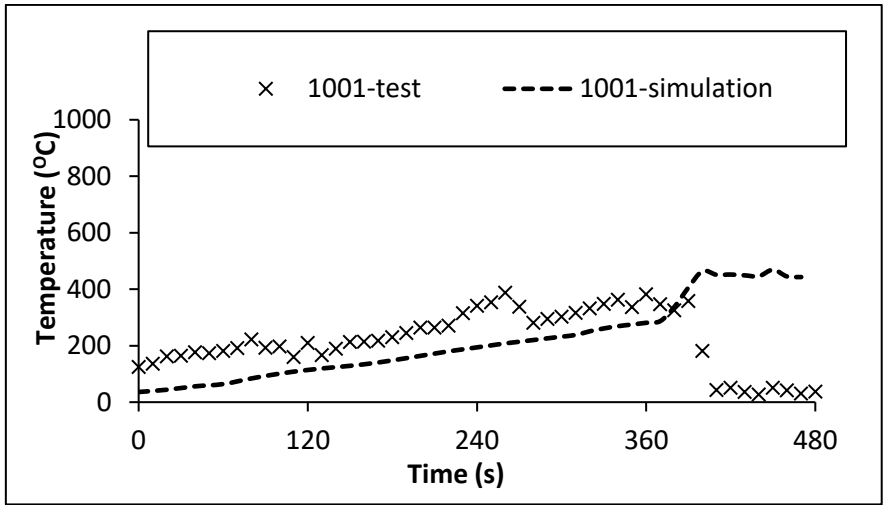

(a)

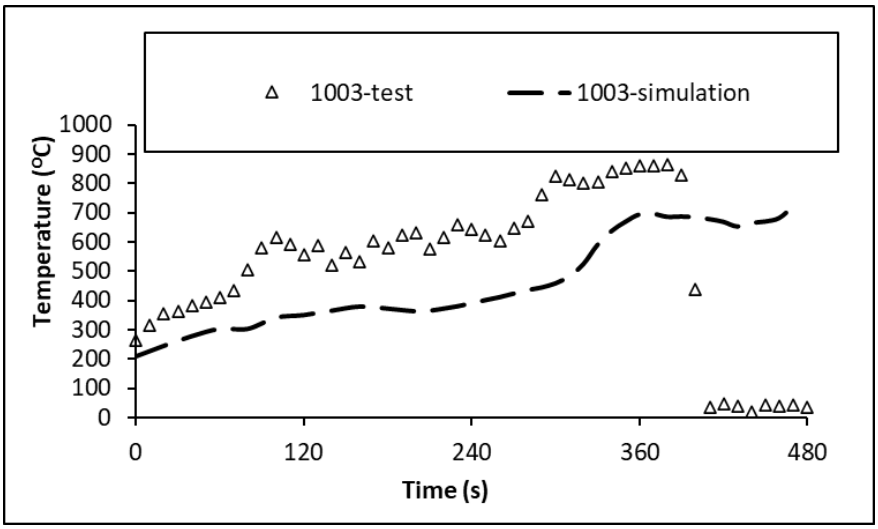

(b)

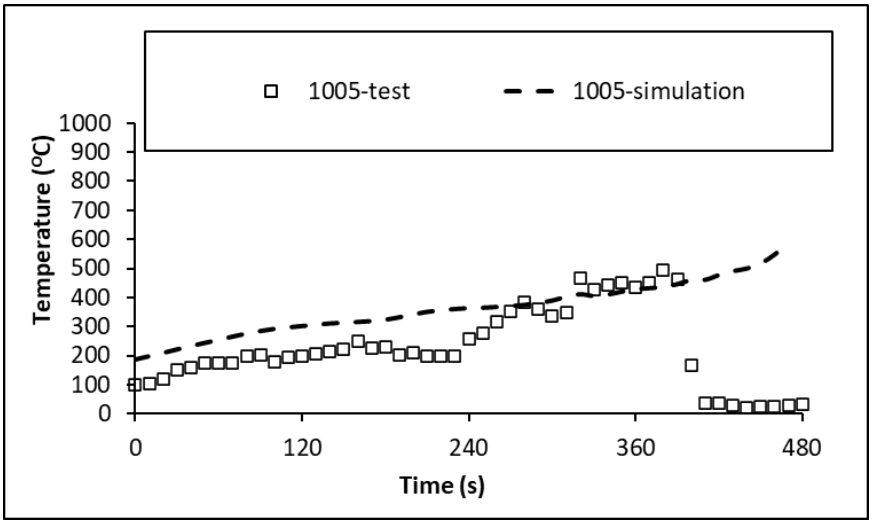

(c)

Fig. S17. Measured and predicted temperatures at external level 1 thermocouples (a) 1; (b) 3 and (c) 5.

S6 Impact of cavity size on temperatures

As reported in Section 5.2 of the main paper, for DCLG test 1 with a cavity size of 0.05 m (as in the DCLG BS 8414 test, and identified as Scenario 1) and with a wider cavity of 0.15 m (identified as Scenario 2), both cladding systems are predicted to fail at almost the same time (360 s) due to the flame rising beyond the top of the facility (Criterion 3) [S1]. As noted in the main paper (see Section 5.2 of [S1]) and depicted in Fig. S18a, up to this time, there are no significant differences in the external temperatures for both cavity widths at Level 2. Furthermore, up until this time, the internal cavity temperatures at Level 2 are also very similar, with the average temperature in the narrow cavity (0.015 m) being slightly higher (see Fig. S18b).

However, after approximately 360 s and up to approximately 730 s (when most of the cladding is burnt off in the wider cavity case as depicted in Fig 12b in [S1]), the average cavity temperature in the wide cavity case exceeds that in the narrow cavity case, by as much as 108 ^{O}C (see Fig. S18b). This higher average cavity temperature promotes the greater surface flame spread rates noted for both the cladding and insulation in the wider cavity case (see Section 5.2 of [S1]).

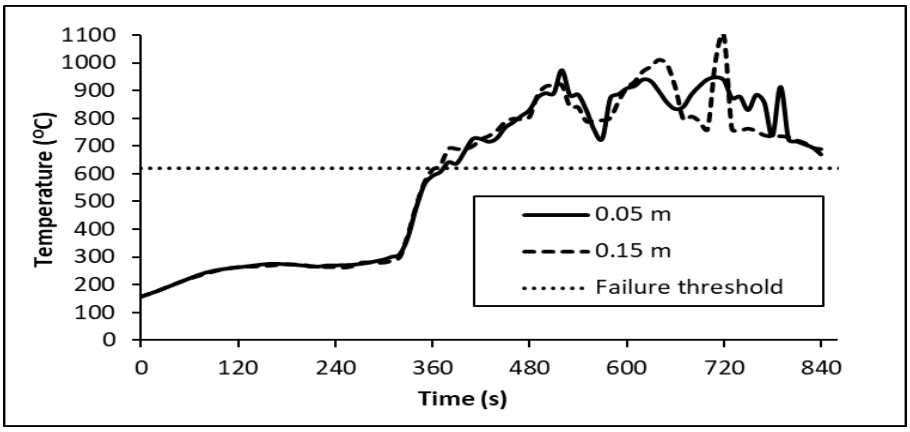

(a) Predicted maximum external temperatures at Level 2

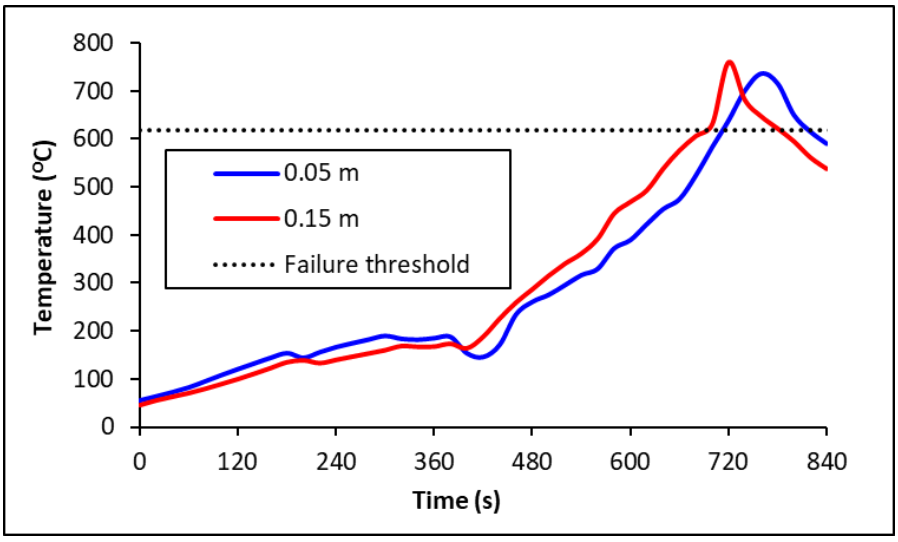

(b) Predicted average cavity temperatures at Level 2

Fig. S18. Comparison of the predicted (a) maximum external temperatures and (b) average cavity temperatures, in the simulation of DCLG BS 8414 test 1 (i.e., Scenario 1 with a cavity size of 0.05 m) and the simulation of this test with an enlarged cavity size (i.e., Scenario 2 with cavity size of 0.15 m).

While the two cladding systems are predicted to fail at almost the same time (360 s) due to the flame rising beyond the top of the facility (Criterion 3), there is a significant difference in the amount of cladding material burnt off at 730 s. As seen in Fig. 12 of the main paper [S1], almost all the ACM panels on the main wall are burnt off (white area) in scenario 2 (0.15 m cavity) at 730 seconds; but the burnt off area in scenario 1 (0.05 m cavity), is approximately only two thirds of that for scenario 2. The simulations suggest that for the case with the larger cavity (i.e., scenario 2) the fire spreads more rapidly on the cladding both vertically and laterally than for the case with the smaller cavity (i.e., scenario 1).

To further explore this behaviour, the lateral and vertical flame spread rates on the cladding for both narrow and wide cavities are estimated from the simulations. The flame spread is determined by the location of the predicted combustion front. However, these flames spread rates are difficult to quantify as they vary across the entire face of a panel and potentially from panel to panel. Furthermore, when estimating both the lateral and vertical flame spread rates the lowest panel locations (i.e., panels 1C and 1D in Fig. 1 of main paper [S1]) are not considered as the flame spread rates on these panels are expected to be dominated by the spill plume arising from the fire chamber immediately below the panel.

To characterise the lateral flame spread rate associated with the different cavity sizes, the centre line across the middle panels on the main wall (i.e., panels 2C and 2D in Fig. 1 of main paper [S1]) were selected. This line is located 5.6 m above the floor (3.6 m above the top of the fire chamber) representing a length of 2.04 m. To characterise the vertical flame spread rate, a vertical line on the centre top two panels of the main wall (i.e., panels 2C and 3C in Fig. 1 of main paper [S1]) 0.2 m to the left of the middle vertical panel gap was selected. The length of the vertical line on ACM panel 2C was 2.23 m and for ACM panel 3C the line measured 1.74 m. An average flame speed along these lines is then estimated from the time that the panel first ignites to when the entire length of the measuring line on the panel is ignited.

For the narrow cavity (0.05 m), the average lateral flame spread rate on the cladding was estimated to be 0.010 m/s while for the wide cavity it was estimated to be 0.013 m/s (i.e., 30% faster). In addition, it is important to note that the cladding at the measuring height first ignites after 460 s in the wide cavity and 483 s in the narrow cavity. Thus, in the wide cavity case, the lateral flame speeds are measured at a time of lower HRR from the wood crib fire.

For the narrow cavity (0.05 m), the average vertical flame spread rates on cladding panels 2C and 3C were estimated to be 0.007 m/s and 0.006 m/s respectively while for the wide cavity (0.15 m), they were estimated to be 0.008 m/s (i.e., 14% faster) and 0.008 m/s (i.e., 33 % faster) respectively.

Comparing the relative magnitudes of the predicted vertical and lateral flame spread rates is not straightforward. The lateral flame spread is progressing in two directions i.e., left and right, whereas the vertical is progressing essentially in a single direction i.e., upwards. Furthermore, the cladding along the horizontal line is first ignited some 230 s after the vertical line is first ignited, and virtually all of the horizontal line is covered in the flames from the spill plume for the entire duration of the measurement, while the vertical line is progressively exposed to flame.

The faster lateral and vertical fire spread rates for the wide cavity compared to the narrow cavity case is the result of the higher average cavity temperatures in the wider cavity after the cladding system fails i.e., 360 s (see Fig. S18b). Thus, while both the narrow and wide cavity

case are determined to fail the BS 8414 test at around the same time, and for the same reason, the wider cavity case presents a significantly more hazardous situation, as both the average lateral and vertical flame spread rates are greater.

S7 Impact of the top window pod

In the DCLG BS 8414 tests, aluminium pods were installed on the top and at the two sides of the combustion chamber [S7]. The window pod extends approximately 0.03 m beyond the front face of the finished cladding system. The lowest horizontal barrier is just above the top window pod. The top window pod is still intact after the termination of the fire in DCLG BS 8414 test 1. Therefore, the cavity of the cladding system is actually protected by the top window pod and its adjacent horizontal barrier. Interestingly, in the Grenfell Tower cladding system, there was no such window pod beneath the cladding (although the ACM cassette arrangement used in Grenfell would have offered some additional protection however, this would be much less than that provided by the window pod). It is unclear why these aluminium barriers were included in the DCLG tests as they clearly provide additional protection to the cavity and the ACM panels.

The impact of the window pod on fire development is investigated by a simulation scenario which is the same as DCLG test 1 but with the top aluminium pod removed. It is noted that both configurations are predicted to fail the BS 8414 test due to flames extending beyond the top of the test facility (criterion 3). For the tested configuration, failure is predicted to occur at 360 s, while for the modified configuration (with the removal of the Aluminium window pod), failure occurs after 300 s i.e., 60 s sooner.

Due to the activation of barrier intumescent, it is not surprising that the removal of the top window pod has minor impact on the predicted cavity temperatures. However, the ignition of the ACM panel in the scenario without the top pod occurs at 160 s, some 90 s earlier than that in the scenario with the window pod present. At 395 s, with the window pod present, the predicted burning area is limited to the lower ACM panel, while in the scenario with the removal of the window pod, the ACM panel around the horizontal gaps (between the top and middle panels) has been ignited (Fig. S19). Furthermore, the burnt off area in the latter scenario is approximately twice of that in the former scenario.

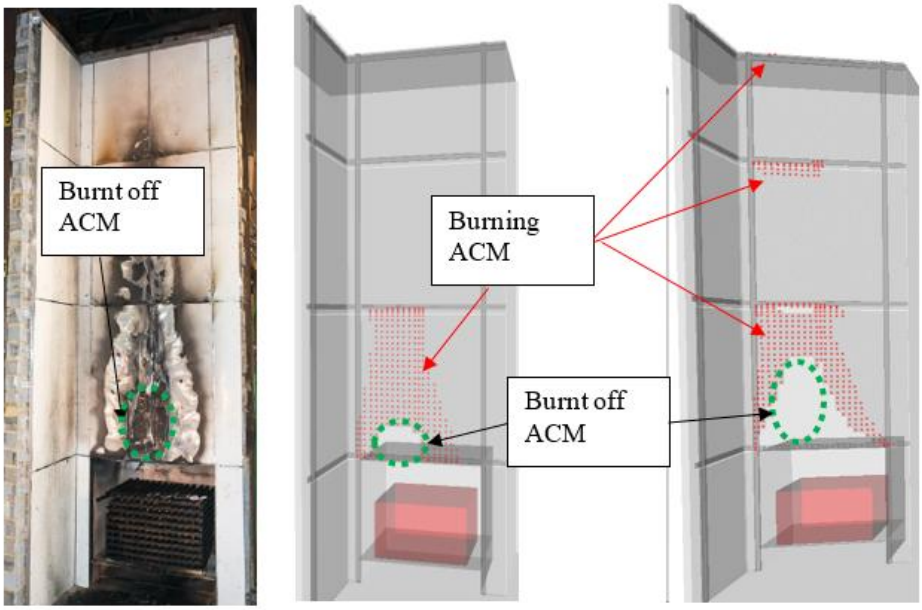

Fig. S19. The final burnt locations in DCLG test1 (left); the predicted ACM burning locations (red dots) and the burnt off locations at 395 s into the simulation scenario the same as the fire test (with the window pod, middle) and in the simulation scenario without the window pod (right).

S8 Material property sensitive analysis

As noted in Section 3.3, Table 2 of the main paper [S1], some of the material thermal properties for the materials in the DCLG fire tests were not provided in the experimental reports [S7] and so values from similar materials derived from the literature were used in the analysis. In this section, the sensitivity of simulation outcomes to changes in material thermal properties are analysed. Amongst some of the unknown parameters are the precise value for the specific heat of PIR used in DCLG test 1, the density for FR PE used in DCLG test 3 and the conductivity of phenolic foam used in DCLG test 7. To explore model sensitivity to these parameters, the specific heat of PIR was increased by 52%, the density of FR PE was increased by 37% and the conductivity of phenolic foam was increased by 50%.

The specific heat of PIR used in the DCLG test 1 simulation was 1100 J/kgK. In this sensitivity study the specific heat is increased to 1670 J/kgK (i.e., by 52%). As seen in Fig. S20, almost identical external level 2 and cavity temperatures are produced by the two PIR specific heat cases. Furthermore, the main conclusions of the simulations i.e., the predicted pass/fail status of the BS 8414 test and the criterion that caused the failure are not altered.

The density of FR PE used in DCLG test 3 simulation was 925 kg/m^3 [S1]. In this sensitivity study the density is increased to 1265 kg/m^3 (i.e., by 37%). Generally, the higher FR PE density leads to a delay in the development of the external cladding fire. The time for the rise of the external level 2 temperature to exceed 600 ^{O}C is 1195 s using the lower density (i.e. 925 kg/m^3) and 1430 s when the higher density (i.e., 1265 kg/m^3) is used, a delay of 19.7% (see Fig. S21). While a relatively large change, this delay does not alter the conclusions of the simulation, nor does it change the pass/fail status. Furthermore, there are insignificant differences in the cavity temperature throughout the simulation.

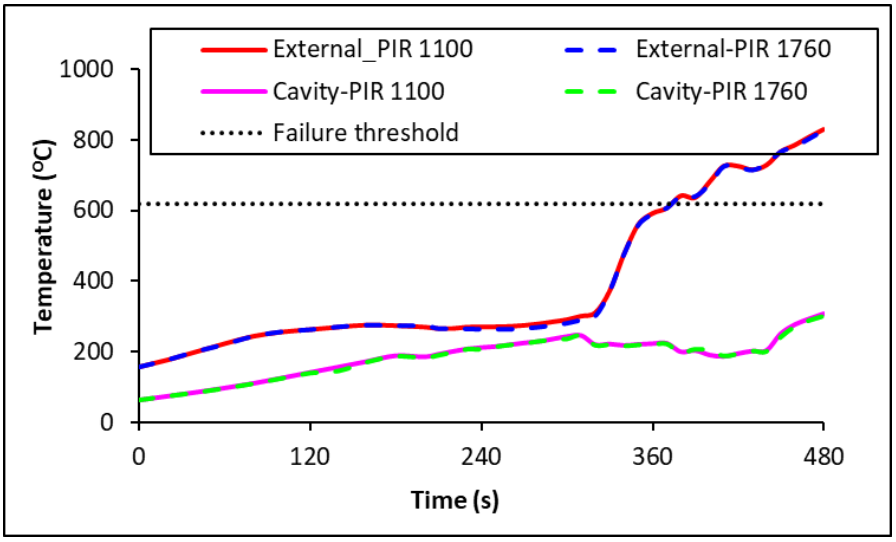

Fig. S20. Comparison of Level 2 external and cavity temperatures for simulations using specific heat for PIR of 1100 J/kgK and 1670 J/kgK in BS 8414 DCLG test 1.

However, DCLG test 3 failed due to the external flame exceeding the height of the rig. The time for this failure to occur is 1310 s using the lower density (i.e., 925 kg/m^3) and 1440 s using the higher density (i.e., 1265 kg/m^3), a delay of 9.9%. Thus, the test is predicted to fail at approximately the same time regardless of the precise value for the density, and so does not change the conclusions of the analysis. This demonstrates that a 37% change in the value of the density of FR PE within the simulations does not result in significant changes in predicted temperatures, the main conclusions of the simulations, the predicted pass/fail status of the BS 8414 test or the criterion that caused the failure.

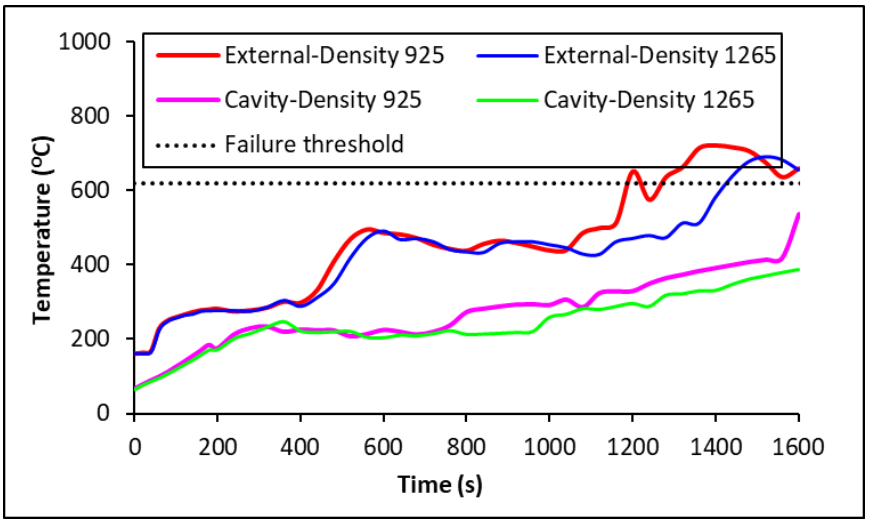

Fig. S21. Comparison of Level 2 external and cavity temperatures for simulations using FR PE densities of 925 kg/m^3 and 1265 kg/m^3 in BS 8414 DCLG test 3.

The conductivity of phenolic foam used in DCLG test 7 simulation was 0.02 W/mK [S1]. In this sensitivity study, the conductivity is increased to 0.03 W/mK (i.e. by 50%). Generally, the higher phenolic foam conductivity leads to a slight delay in the development of the external cladding fire. The time for the rise of the level 2 temperature to exceed 600 ^{O}C is 1300 s using the lower conductivity (i.e., 0.02 W/mK) and 1320 s when the higher conductivity (i.e., 0.03 W/mK) is used, a delay of 1.5% (Fig. S22). This delay does not change the conclusions of the simulation, nor does it change the pass/fail status. Furthermore, there are no significant

differences in cavity temperature between the two conductivity cases throughout the simulations, with the exception of a local peak temperature at 1280 s. However, DCLG test 7 failed due to the external flame exceeding the height of the rig. The time for this failure to occur is 1360 s using the lower conductivity (i.e., 0.02 W/mK) and 1380 s using the higher conductivity (i.e., 0.03 W/mK), a delay of 1.5%. Thus, the test is predicted to fail at approximately the same time regardless of the precise value for the conductivity, and so does not change the conclusions of the analysis. This demonstrates that a 50% change in the value of the conductivity of phenolic within the simulations does not result in significant changes in predicted temperatures, the main conclusions of the simulations, the predicted pass/fail status of the BS 8414 test or the criterion that caused the failure.

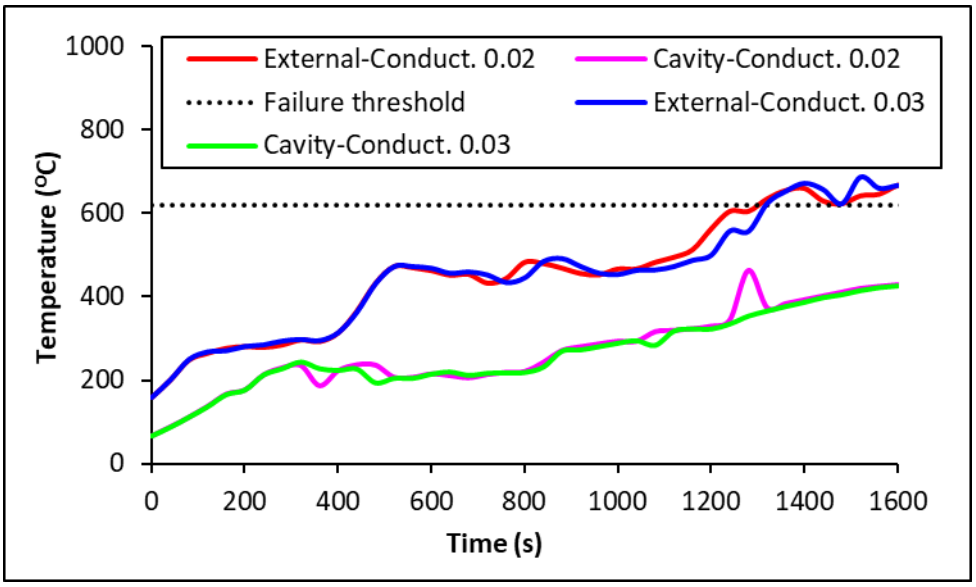

Fig. S22. Comparison of Level 2 external and cavity temperatures for simulations using phenolic conductivities of 0.02 W/mK and 0.03 W/mK in BS 8414 DCLG test 7.

Thus, while it is preferable to use the correct values for the material properties, if available; using reasonable approximations to material properties based on those for similar materials, with appropriate sensitivity analysis, is likely to produce acceptable results.

References

[S1] Wang Z., Jia F, Galea, E.R. and Ewer, J., CFD simulation of the BS 8414 test for Cladding Applications, Fire Safety Journal (104366), published online 22 Feb 2025, https://doi.org/10.1016/j.firesaf.2025.104366.

[S2] BS 8414-1:2015+A1:2017. Fire performance of external cladding systems – Part 1: Test method for non-loadbearing external cladding systems applied to the masonry face of a building. British Standards Institution. London, 2017.

[S3] BS 8414-1, Fire performance of external cladding systems – Part 1: Test method for non-loadbearing external cladding, BSI Standards Limited, 2020.

[S4] Bjegović, D., Pečur, I. B., Milovanović, B., Jelčić Rukavina, M. ., Alagušić, M., Comparative full-scale fire performance testing of ETICS systems, GRAĐEVINAR, 68 (5), 357-369, 2016. doi: https://doi.org/10.14256/JCE.1347.2015

[S5] Cladding Approval, A review and investigation of potential shortcoming of the BS 8414 standard for the approval of cladding system such as those commonly used on tall buildings, Fire Protection Association, 22 February 2018.

[S6] Private Communication, email from Prof Richard Hull, University of Central Lancashire, UK, 18 July 2019.

[S7] BRE Global Client reports , report number B137611-1037 (DCLG test 1; DCLG test 2; DCLG test 3; DCLG test 4; DCLG test 5; DCLG test 6; DCLG test 7, DCLG test 8), BRE Global, UK, 2017.

[S8] McKenna S.T., Jones N., Peck G, et al., Fire behaviour of modern façade materials – Understanding the Grenfell Tower fire, Journal of Hazardous Materials, Vol. 368, No. 15, pp. 115-123, 2019. https://doi.org/10.1016/j.jhazmat.2018.12.077